The Astrophysical Journal, 680: L149–L152, 2008 June 20

HARD X-RAYS ASSOCIATED WITH TYPE III RADIO BURSTS

S. Christe, S. Krucker, and R. P. Lin[1]
Space Sciences Laboratory, University of California at Berkeley, Berkeley, CA; schriste@ssl.berkeley.edu, krucker@ssl.berkeley.edu, rlin@ssl.berkeley.edu
Received 2008 February 12; accepted 2008 May 9; published 2008 May 27

ABSTRACT

During a period of 12 minutes on 2002 July 19 14:23–14:35 UT, the WAVES instrument on *WIND* observed six interplanetary type III radio bursts, one approximately every 2 minutes, and each was accompanied by a weak hard X-ray (HXR) burst (12–15 keV) observed by *RHESSI*. The radio bursts are observed up to 150 MHz with some up to 600 MHz. Simultaneous observations by *TRACE* show jetlike eruptions emanating from the region of HXR emission. The observed HXRs are inconsistent with emission from the escaping type III–producing nonthermal electrons. We suggest that the type III acceleration process may be associated with an explosive release of $\lesssim 5 \times 10^{26}$ ergs in the form of a "superhot" (26 MK) thermal plasma in the corona, an energy comparable to that associated with the type III–producing electrons.

Subject headings: Sun: activity — Sun: corona — Sun: flares — Sun: radio radiation — Sun: X-rays, gamma rays

Online material: color figures

1. INTRODUCTION

Hard X-ray (HXR) bursts and type III radio bursts are two of the most common solar impulsive emissions produced by energetic electrons through bremsstrahlung and beam-plasma interactions, respectively. HXR bursts are commonly observed in association with solar flares, even in microflares (Lin et al. 1991, 2001; Krucker et al. 2002). Imaging reveals that the HXR emission comes predominantly from the chromospheric footpoints of flare loops, where the ambient densities are high enough for the electrons to rapidly lose their energy to collisions. At lower energies, thermal HXRs are observed in the flare loop, which is filled with tens of millions of degree plasma.

Type III radio bursts are characterized by a rapid drift from high to low frequency. Hypothesized by Wild et al. (1954) to be caused by escaping energetic electrons traveling through the corona, these electrons are often also detected in situ, near 1 AU, in impulsive electron events that occur $\gtrsim$1000 events per year near solar maximum over the whole Sun (see Lin 1985 for review). Bump-on-tail electron distributions are often observed at the onsets of these impulsive events due to velocity dispersion—i.e., the faster electrons run ahead of the slow ones. Such distributions are unstable to the growth of Langmuir waves that in turn can interact with density fluctuations or with other waves to produce radio emission near the local plasma frequency or its harmonic. Unstable electron distributions with simultaneous bursts of Langmuir waves and type III radio emission have been observed (Lin et al. 1981), confirming Wild's hypothesis. These escaping electrons will produce also HXR bremsstrahlung emission although at a very low rate due to the low density of the corona.

De Jager (1963) was the first to suggest that type III– and HXR-producing energetic electrons originate from a common accelerator. He postulated two populations—upward-directed electrons that generate the type III radio burst and downward-directed electrons that produce the HXR emission. Subsequent studies confirmed the relationship between HXR-producing flare electrons and type III–producing electrons. Kane (1981) found that 3% of type III bursts occurred with a simultaneous HXR burst (increasing systematically with the start frequency of the radio bursts), although 20% of impulsive HXR bursts have near simultaneous type IIIs. Aschwanden et al. (1990) found that 31% of a large sample of HXR peaks were associated with type III bursts (at around 300 MHz). Benz et al. (2005) found type III bursts are the most frequent radio emission found during HXR flares (although only a 33% association) and that they occur preferentially during the peak and impulsive phase. Type III radio bursts have also been shown to be closely associated with coronal jets observed in soft X-rays (Aurass et al. 1994; Kundu et al. 1995; Raulin et al. 1996).

Here we present high-sensitivity *Reuven Ramaty High Energy Solar Spectroscopic Imager* (*RHESSI*; see Lin et al. 2002) observations of six type III bursts with simultaneous HXR emission that occurred in a 12 minute period and discuss the implications for the origin of type III bursts.

2. OBSERVATIONS

RHESSI's nine cryogenically cooled germanium detectors (GeDs) detect photons from 3 keV up to ~17 MeV with a spectral resolution of ~1 keV (FWHM) up to ~300 keV (Smith et al. 2002). *RHESSI*'s high sensitivity at low energies, compared to previous instruments, is due to its use of automatic shutters. Most previous solar HXR instruments used thick windows in order to block the intense thermal fluxes observed in large flares while *RHESSI* uses movable shutters that are automatically inserted but only during large flares. With the shutters out, *RHESSI*'s sensitivity at 10 keV is up to 100 times higher than previous HXR spectrometers (e.g., Krucker et al. 2002). Imaging with spatial resolution down to ~2.3″ with a full-Sun (>1°) field of view is provided by bigrid rotating modulation collimators in front of each GeD (Hurford et al. 2002). The associated radio observations are from the WAVES instrument on *WIND* (20 kHz–12 MHz, 16 s resolution; see Bougeret et al. 1995), Phoenix-2 (100 MHz–4 GHz, 0.1 s resolution; see Messmer et al. 1999), and the radio spectrometer at Potsdam (40–800 MHz).

Between the time that *RHESSI* came out of Earth's shadow at 14:23 and went into the South Atlantic Anomaly at 14:35 UT on 2002 July 19, six interplanetary type III radio bursts were observed

[1] Department of Physics, University of California at Berkeley, Berkeley, CA.

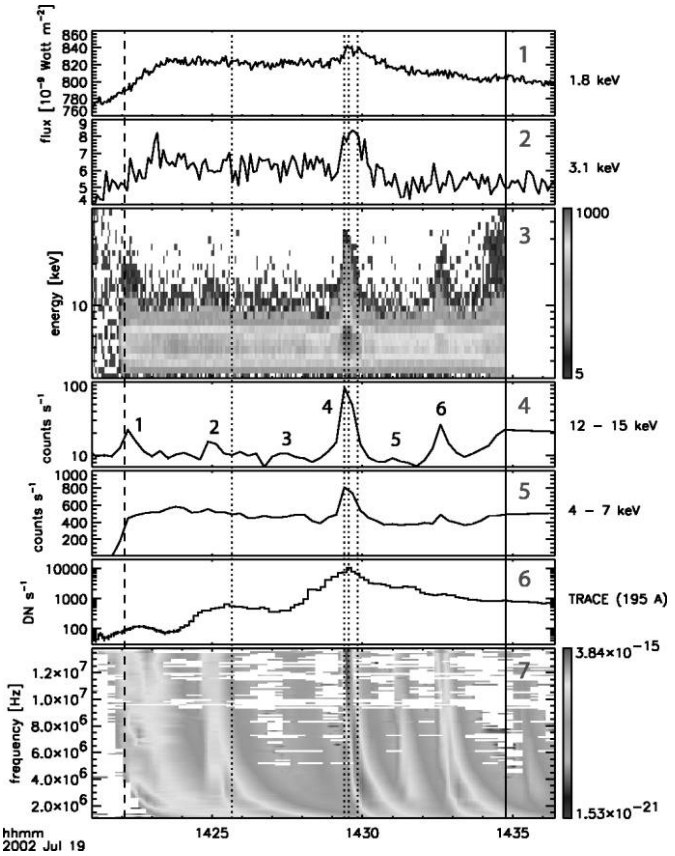

FIG. 1.—Overview plot of the 2002 July 19 type III series. *Panels 1 and 2*: *GOES* 1–8 Å (1.6 keV) and 0.5–4 Å (3.1 keV) light curves in a linear scale. *Panel 3*: *RHESSI* spectrogram plot, nighttime background-subtracted. *Panel 4*: *RHESSI* 12–15 keV light curve (nonthermal). *Panel 5*: *RHESSI* 4–7 keV light curve (thermal). *Panel 6*: *TRACE* light integrated over the region shown in Fig. 3. *Panel 7*: Radio spectrogram from WAVES on *WIND*. The dashed line delimits the end of eclipse for *RHESSI*. The solid line indicates the South Atlantic Anomaly during which *RHESSI* data is unavailable. The dotted lines represent times at which *RHESSI* images were created (see Fig. 3). [*See the electronic edition of the Journal for a color version of this figure*.]

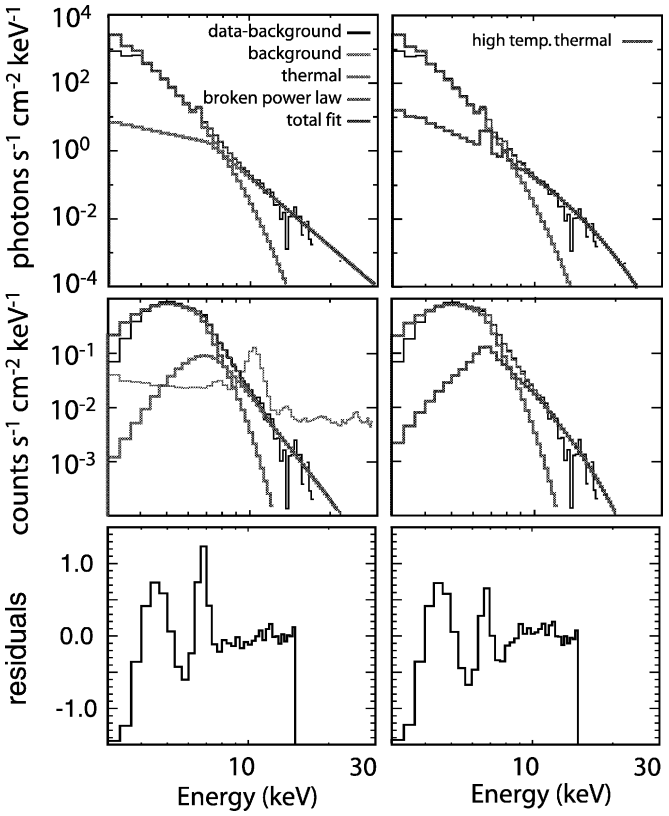

FIG. 2.—*RHESSI* spectra of the summed small events (bursts 1, 2, 3, and 5) including solar background. At low energies, the solar background is best fit with a thermal spectrum with a temperature of ~9 MK and emission measure of 2×10^{47} cm^{-3}. The light gray line in the middle left panel represents the instrumental background. The thermal plus nonthermal fit are on the left, and the double thermal fit is on the right. The photon spectrum (*top*) is shown above the count spectrum (*middle*). The nonthermal slope was found to be steep with a spectral index of 7.5 ± 0.8. The temperature of the high thermal fit was found to be ~26 MK with an emission measure of 2×10^{44} cm^{-3} per event. The bottom panels show the normalized residuals. [*See the electronic edition of the Journal for a color version of this figure*.]

below 14 MHz by WAVES on *WIND* (see Fig. 1). Phoenix-2 and Potsdam detected these same events up to 150 MHz, with two bursts (bursts 2 and 4) extending to ~600 MHz. A weak X-ray brightening was observed by *RHESSI* between 12 and 15 keV simultaneous with each of the type III bursts, within the 16 s time resolution of WAVES . Considering the flare rate (~90 flares per day; see Christe et al. 2008) and the interplanetary type III rate (~10 per day) for 2002 July, the chance coincidence rate is 0.05 events for a 20 minute period, which cannot explain the six coincident events observed here. At lower energies (4–7 keV), only the two strongest events (bursts 4 and 6) show any emission above the HXR background. Furthermore, these are the only two events detected by *GOES* (*GOES* class <A4 above a B8 background), but they are not listed in the NOAA Space Environment Center solar event reports. Based on observations discussed below, we conclude that events 4 and 6 are "standard" HXR events related to impulsive electrons (see Krucker et al. 2007) with flarelike nonthermal HXR, thermal soft X-ray characteristics, and a simultaneous release of electrons into interplanetary space.

Due to inadequate statistics in the small events (bursts 1, 2, 3, and 5), they were summed together to obtain the photon spectrum shown in Figure 2. Spectral fits were made using OSPEX, an updated version of the SPEX analysis package (Schwartz 1996). The *RHESSI* nighttime background was subtracted from this spectrum. A solar background is observed in the 4–7 keV light curve as soon as *RHESSI* enters daylight (see Fig. 1). The spectrum of this background is modeled well by thermal bremsstrahlung emission with an emission measure of $(2 \pm 0.2) \times 10^{47}$ cm^{-3} and a temperature of 7.8 ± 0.5 MK. This solar background is nearly constant over the 12 minutes considered here with no significant increase at the times of events 1, 2, 3, and 5; if this background is subtracted, then no low-energy (<7 keV) emission is present during these events.

A model consisting of a single-temperature thermal distribution (to model the background) and a nonthermal broken power law, with the power-law index set to 1.7 for energies below the break energy (this approximates the photon spectrum turnover assuming a sharp cutoff in the electron spectrum), was fit to the summed spectrum (Fig. 2, *left*). Compared to the solar background, no statistically significant increase in emission is seen for these events below ~12 keV; above this energy, a steep spectrum is observed with a negative power-law index of 7.5 ± 0.8 with a cutoff of ~8 keV. This fitted cutoff is significantly below the value at which the thermal and nonthermal spectrum deviate significantly (~12 keV) but provides the best fit to the data, suggesting that some nonthermal emission may be hidden below the thermal emission. For all the following calculations, however, the more conservative 12 keV cutoff is used. The associated average thick-

target nonthermal electron energy per burst is $\sim 3 \times 10^{28}$ ergs using a cutoff energy of 12 keV and the average event duration of 20 s. This steep spectrum can also be fit by a high-temperature thermal spectrum with temperature of 26 MK and an emission measure of 2×10^{44} cm^{-3} per event (Fig. 2, *right*). Since no imaging is available for these small events, the (instantaneous) thermal energy cannot be calculated without some assumptions (see § 3).

For the larger bursts, events 4 and 6, *RHESSI* images show emission originating from N17° W50.5° on the western edge of the NOAA active region 0030. Imaging is not possible for any of the other events. Nançay radio images (K.-L. Klein 2002, private communication) show that all of the type III bursts are located above this active region. This suggests that the smaller events are located in the same active region. *Transition Region and Coronal Explorer* (*TRACE*) extreme-ultraviolet (EUV) images ($\sim 1''$ spatial resolution and a field of view of 8.5×8.5 arcmin^2) at 195 Å (Fe XII, 0.5–2 MK) covering this region are available for the entirety of the *RHESSI* observations (see Fig. 3). These were coaligned to a few arcseconds with the *RHESSI* images, using *Solar and Heliospheric Observatory* EIT for pointing knowledge. Before 14:27:49 UT, *TRACE* images show complex background emission (see Fig. 3, *top left*). A loop structure is clearly apparent for the remainder of the observations. At 14:25:40 UT, directly after the first fully observed type III burst occurs (event 2), *TRACE* background-subtracted images show increased emission along a line extending northwest from the southernmost footpoint. This emission persists while the loop brightens. During the impulsive phase of event 4, *RHESSI* images (processed by the PIXON algorithm; Metcalf et al. 1996) show both a nonthermal (12–30 keV) and thermal (3–10 keV) source coincident with the southern footpoint (Fig. 3, *top right*). Less than 9 s later, *RHESSI* images show only a thermal source, and two EUV jetlike eruptions are seen in *TRACE* (14:29:33 UT; Fig. 3, *bottom left*). The jets propagate along the line of increased emission previously mentioned. The observed jets have sizes of $\sim 1 \times 10^4$ km with an average lifetime of ~44 s. The centroids of the jets are found to travel at apparent speeds of ~100 km s^{-1}. Similar EUV jets associated with type III radio bursts have been observed by Chae et al. (1999) and by Raulin et al. (1996) in soft X-rays. A linear extrapolation of the jet propagation direction lines up directly with the radio sources observed by the Nançay Radioheliograph (150–450 MHz) approximately 300″ above the region of interest. *TRACE* emission, spatially integrated over the loop area, can be seen in Fig. 1. The first three events are each accompanied by an increase in *TRACE* emission. During the decay phase, *RHESSI* images (3–10 keV) outline the *TRACE* loop structure (Fig. 3, *bottom right*). The thermal emission of event 4 shows a similar structure.

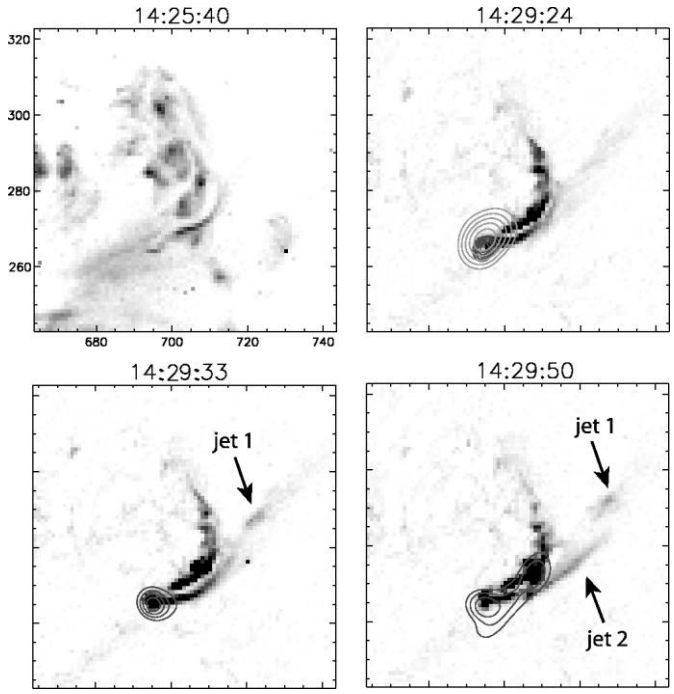

FIG. 3.—*RHESSI* images overlaid on *TRACE* Fe XII (195 Å; pre-event background-subtracted) images. The *RHESSI* images were processed by the PIXON algorithm. Note that the PIXON algorithm tends to overestimate source sizes for images with low counts. The top left panel shows the pre-event background. The next panel (*top right*) shows the emergence of a linear structure coincident with a loop brightening and *RHESSI* nonthermal (*large source*) and thermal HXR (*small*) sources. Two jets are observed to emanate from the location of the *RHESSI* thermal and nonthermal flux. The bottom two panels show only thermal HXR sources. [*See the electronic edition of the Journal for a color version of this figure.*]

3. DISCUSSION

We first consider whether the observed 12–15 keV emission for events 1, 2, 3, and 5 is the result of the escaping type III–producing electrons emitting thin-target nonthermal bremsstrahlung. An electron traversing an ionized plasma suffers energy losses due to Coulomb collisions with ambient electrons at a rate given by $dE/dx = -Cn/E$ (Trubnikov 1965), where n is the ambient density and $C = 2\pi e^4 \ln\Lambda \approx 3.3 \times 10^{-18}$ keV^2 cm^2. Integrating over n gives the minimum energy necessary for an electron to traverse a column depth, $K = \int n\, dx$ (Lin 1974),

$$E_{\min} = \sqrt{2KC}. \quad (1)$$

Thus, for thin-target emission, the electron energy must be significantly larger than $E_{\min}$, while electrons with $E < E_{\min}$ are lost. Using equation (1), the Baumbach-Allen model corona (e.g., Cox 2000) and the maximum observed frequency of the associated type III emission (150 MHz) as a measure of the starting plasma density ($f_p = 9000\sqrt{n}$ in cgs units) gives $E_{\min} \simeq 4$ keV. Thus, greater than ≈10 keV escaping electrons emit thin-target HXRs.

For a thin-target X-ray spectrum observed at 1 AU of $F(h\nu) = A(h\nu)^{-\gamma}$ (photons cm^{-2} s^{-1} keV^{-1}), the required instantaneous electron distribution, dn/dE (electrons s^{-1} keV^{-1}), is given by (Lin 1974; corrected for a missing factor of π)

$$\frac{dn_e(E)}{dE} = 1.21 \times 10^{42} \gamma(\gamma - 1)^2 \beta(\gamma - 1/2,\ 3/2)\, \frac{AE^{-\gamma+1/2}}{n}, \quad (2)$$

where n is the density in cm^{-3}, E is energy in keV, and $\beta(x, y)$ is the Beta function. In the thin-target spectrum, the observed emission requires an instantaneous electron rate of 3.8×10^{37} electrons s^{-1} above 10 keV and an electron power-law index of about −7.0. If we assume the X-ray–emitting region dimension is the coronal scale height (5×10^9 cm), then the total number of accelerated electrons required in order to sustain emission over the observed timescale (~20 s) is ≈10^{39} electrons.

For the presented events, no in situ solar impulsive electron events were detected near 1 AU by the 3D Plasma and Energetic Particle instrument (Lin et al. 1995) on the *WIND* spacecraft. The active region would normally be connected to the vicinity of the Earth by the nominal Parker spiral interplanetary magnetic

field (IMF), but the IMF was strongly distorted by an interplanetary disturbance between ~15:00 and 17:00 UT, when the escaping electrons should have arrived. Typical impulsive electron events release $\sim 10^{33}$ electrons between 10 and 100 keV to the interplanetary medium (Lin 1974) with a spectral power-law index of -2.0 (Lin et al. 1982), completely inconsistent with our derived thin-target spectrum. We therefore conclude that the observed HXRs are inconsistent with thin-target emission from escaping electrons.[2] Krucker et al. (2007) studied a set of 16 events with associated HXR emission, type III bursts, and in situ electrons observed at Earth and found that the photon and spectral indices were linearly related through $\gamma \propto \delta$. The difference between the HXR spectral index and a typical impulsive electron event presented here is too large to be consistent with this relation even considering the softest impulsive events presented by Krucker et al. (2007), which suggest that these events are different.

Events 1, 2, 3, and 5 are similar to microflares (Krucker et al. 2002; Benz & Grigis 2002; Christe et al. 2008; Hannah et al. 2008) in that they have steep nonthermal spectra (spectral slope of -7.5), similar total nonthermal fluxes, and nonthermal durations although little or no thermal heating is observed due to a high solar background. If we assume thick-target emission, the average nonthermal electron energy in these events is 3×10^{28} ergs, requiring 8×10^{35} electrons above 12 keV. These values are similar to typical microflares (see Christe et al. 2008). Interpreting these events as microflares does not explain the close relationship with the type III radio bursts.

As mentioned earlier, a purely thermal model with $T = 26$ MK and EM $= 2 \times 10^{44}$ cm^{-3} also fits the 12–15 keV emission (see Fig. 2). If we assume the density given by the highest frequency type III emission (4×10^9 cm^{-3}, 0.2 $R_\odot$), the thermal energy is $\sim 5 \times 10^{26}$ ergs, and the corresponding volume has a scale size of ~3000 km (4″). For higher densities, the thermal energies are smaller ($\lesssim 5 \times 10^{26}$ ergs) and the size scale larger ($\gtrsim 4''$). This energy is comparable to the *total* energy (>10 keV) contained in the electrons in a typical type III burst-related impulsive event observed at 1 AU.

[2] These results also imply that *RHESSI* is unlikely to detect thin-target HXRs from typical type III–producing electrons except possibly for partially disk-occulted events where purely coronal emissions are seen (Krucker et al. 2008).

4. CONCLUSIONS

The radio and X-ray observations presented here suggest a close relationship between type III radio bursts and HXR emission. Type III radio bursts are known to be signatures of escaping electrons. HXRs are usually associated with accelerated energetic electrons trapped in coronal loops. Considering the smallest events, the simplest scenario that the type III–producing escaping electrons produce the HXR emission directly is not consistent with the data. The photon spectrum is too steep, and the photon flux is too large. Interpreted as nonthermal thick-target emission, these events show little or no thermal heating, although some may be hidden in the background; therefore, this interpretation cannot be excluded. The steepness of the spectrum suggests that it is not related to the type III–producing electrons and therefore cannot explain the temporal relationship between the two kinds of emission. We therefore suggest that the HXR emission is best interpreted as thermal emission. The radio and X-ray observations suggest an explosive release of $\lesssim 5 \times 10^{26}$ ergs in the corona, with a comparable amount of energy going into a superhot (26 MK) thermal plasma and into 10^{33} accelerated electrons that escape the Sun. We speculate that the type III acceleration process is associated with a superhot thermal plasma. Such superhot signatures have been observed in larger flares (Lin & Schwartz 1987) and may be present in microflares (Benz & Grigis 2002).

This work was supported under NASA grants NAS5-98033, NNM05ZA12H, and NNX07AH76G. The authors would like to thank Arnold Benz for supplying the Phoenix-2 data and Nicole Vilmer along with Karl-Ludwig Klein for access to Nançay Radio Heliograph data. S. Christe would like to thank A. Y. Shih for helpful discussions.

REFERENCES

Aschwanden, M. J., Benz, A. O., & Kane, S. R. 1990, A&A, 229, 206
Aurass, H., Klein, K.-L., & Martens, P. C. H. 1994, Sol. Phys., 155, 203
Benz, A. O., & Grigis, P. C. 2002, Sol. Phys., 210, 431
Benz, A. O., Grigis, P. C., Csillaghy, A., & Saint-Hilaire, P. 2005, Sol. Phys., 226, 121
Bougeret, J.-L., et al. 1995, Space Sci. Rev., 71, 231
Chae, J., Qiu, J., Wang, H., & Goode, P. R. 1999, ApJ, 513, L75
Christe, S., Hannah, I. G., Krucker, S., McTiernan, J., & Lin, R. P. 2008, ApJ, 677, 1385
Cox, A. N. 2000, Allen's Astrophysical Quantities (4th ed.; New York: AIP)
de Jager, C. 1963, Space Sci. Rev., 1, 487
Hannah, I. G., Christe, S., Krucker, S., Hurford, G. J., Hudson, H. S., & Lin, R. P. 2008, ApJ, 677, 704
Hurford, G. J., et al. 2002, Sol. Phys., 210, 61
Kane, S. R. 1981, ApJ, 247, 1113
Krucker, S., Christe, S., Lin, R. P., Hurford, G. J., & Schwartz, R. A. 2002, Sol. Phys., 210, 445
Krucker, S., Kontar, E. P., Christe, S., & Lin, R. P. 2007, ApJ, 663, L109
Krucker, S., Saint-Hilaire, P., Christe, S., White, A., Chavier, D., Bale, S. D., & Lin, R. P. 2008, ApJ, in press
Kundu, M. R., Raulin, J. P., Nitta, N., Hudson, H. S., Shimojo, M., Shibata, K., & Raoult, A. 1995, ApJ, 447, L135
Lin, R. P. 1974, Space Sci. Rev., 16, 189
———. 1985, Sol. Phys., 100, 537
Lin, R. P., Feffer, P. T., & Schwartz, R. A. 2001, ApJ, 557, L125
Lin, R. P., Hurley, K. C., Smith, D. M., & Pelling, R. M. 1991, Sol. Phys., 135, 57
Lin, R. P., Mewaldt, R. A., & van Hollebeke, M. A. I. 1982, ApJ, 253, 949
Lin, R. P., Potter, D. W., Gurnett, D. A., & Scarf, F. L. 1981, ApJ, 251, 364
Lin, R. P., & Schwartz, R. A. 1987, ApJ, 312, 462
Lin, R. P., et al. 1995, Space Sci. Rev., 71, 125
———. 2002, Sol. Phys., 210, 3
Messmer, P., Benz, A. O., & Monstein, C. 1999, Sol. Phys., 187, 335
Metcalf, T. R., Hudson, H. S., Kosugi, T., Puetter, R. C., & Pina, R. K. 1996, ApJ, 466, 585
Raulin, J. P., Kundu, M. R., Hudson, H. S., Nitta, N., & Raoult, A. 1996, A&A, 306, 299
Schwartz, R. 1996, NASA STI/Recon Tech. Rep. N, 96, 71448 (Washington, DC: NASA)
Smith, D. M., et al. 2002, Sol. Phys., 210, 33
Trubnikov, B. A. 1965, Rev. Plasma Phys., 1, 105
Wild, J. P., Roberts, J. A., & Murray, J. D. 1954, Nature, 173, 532